Analysis of ICESat-2 Data Acquisition Algorithm Parameter Enhancements to Improve Worldwide Bathymetric Coverage

James T. Dietrich[1], Ann Rackley Reese[2], Aimée Gibbons[2], Lori A. Magruder[1,3], and Christopher E. Parrish[4]

[1] 3D Geospatial Laboratory, Center for Space Research, Cockrell School of Engineering, University of Texas at Austin, Austin, TX, USA

[2] KBR, Greenbelt, MD, USA

[3] Department of Aerospace Engineering and Engineering Mechanics, Cockrell School of Engineering, University of Texas at Austin, Austin, TX, USA

[4] School of Civil and Construction Engineering, Oregon State University, Corvallis, OR, USA

Corresponding author: James T. Dietrich (james.dietrich@austin.utexas.edu)

Key Points:

- Recent updates to ICESat-2's receiver algorithm parameters have boosted the bathymetric measurement capabilities.
- The new updates allow ICESat-2 to consistently measure bathymetry up to 41 m deep.
- The updates allow ICESat-2 to potentially measure over 6.1 million km^2 of new bathymetry in both coastal and ocean settings.

Keywords: ICESat-2, bathymetry, retrievability

Abstract

A major advance in global bathymetric observation occurred in 2018 with the launch of NASA's ICESat-2 satellite, carrying a green-wavelength, photon-counting lidar, the Advanced Topographic Laser Altimeter System (ATLAS). Although bathymetric measurement was not initially a design goal for the mission, pre- and post-launch studies revealed ATLAS's notable bathymetric mapping capability. ICESat-2 bathymetry has been used to support a wide range of coastal and nearshore science objectives. However, analysis of ICESat-2 bathymetry in numerous locations around the world revealed instances of missing or clipped bathymetry in areas where bathymetric measurement should be feasible. These missing data were due to the ATLAS receiver algorithms not being optimized for bathymetry capture. To address this, two updates have been made to ICESat-2's receiver algorithm parameters with the goal of increasing the area for which ICESat-2 can provide bathymetry. This paper details the parameter changes and presents the results of a two-phased study designed to investigate ICESat-2's bathymetry enhancements at both local and global scales. The results of both phases confirm that the new parameters achieved the intended goal of increasing the amount of bathymetry provided by ICESat-2. The site-specific phase demonstrates the ability to fill critical bathymetric data gaps in open ocean and coastal settings. The global analysis shows that the area of potential bathymetry approximately doubled, with 6.1 million km^2 of new area in which bathymetric measurements may be feasible. These enhancements are anticipated to facilitate a range of science objectives and close the gap between ICESat-2 bathymetry and offshore sonar data.

1 Introduction

NASA's Ice, Cloud, and land Elevation Satellite -2 (ICESat-2) satellite, a follow-on to the original ICESat mission, launched on September 15, 2018. Similar to its predecessor, ICESat-2's primary mission goals focused on cryospheric science (Markus et al., 2017; Schutz et al., 2005), while additional mission objectives included global acquisition of vegetation canopy heights to support terrestrial ecosystem studies (Neuenschwander & Pitts, 2019). ICESat-2 carries a single instrument, ATLAS (Advanced Topographic Laser Altimeter System), a photon-counting lidar that was developed to provide improved along-track resolution and multiple beams to mitigate some operational constraints revealed with the previous mission (Neumann et al., 2019).

Although measurement of bathymetry was not an original mission requirement, there were two design decisions that provided ATLAS with a substantial bathymetric measurement capability: the selection of single photon-sensitive photomultiplier (PMT) detectors and the use of a visible, green (532 nm) laser. These two factors were related, as the only available space-hardened PMTs for ATLAS were optimized for 532 nm. While it was known prior to launch ATLAS would have the potential for bathymetric measurement (Forfinski-Sarkozi & Parrish, 2016), its exact bathymetric measurement performance was difficult to predict. Furthermore, there were no plans, at the time, to develop a dedicated mission data product or any operational requirements around bathymetry retrievals once on-orbit. Post-launch, as the initial ICESat-2 data became available, it was evident that ICESat-2's bathymetric measurement performance exceeded expectations. Multiple studies confirmed the ability to retrieve bathymetry to ~1 Secchi depth, or > 40 m in very clear waters, with typical accuracies on the order of 0.5 m (Albright & Glennie, 2021; Chen et al., 2021; Le Quilleuc et al., 2022; Parrish et al., 2019; Ranndal et al., 2021; Watkins et al., 2023; Zhang et al., 2022). These bathymetric capabilities were soon shown to be of value for a wide range of science uses, from the study of coral reefs and other sensitive marine habitats to assessment of seafloor morphological change (Herrmann et al., 2022; Le Quilleuc et al., 2022; Selamat et al., 2021; Van An et al., 2023). One growing application is the fusion of ICESat-2 bathymetric data with optical satellite imagery to create satellite derived bathymetry (SDB) maps in shallow coastal environments (Babbel et al., 2021; Cao et al., 2021; Ma et al., 2020; Thomas et al., 2022). Because of the bathymetric capabilities, NASA is currently funding the development a new Level-3a data product focused on along-track bathymetry extraction with the designation ATL24.

Despite ICESat-2's notable bathymetric capability, it became apparent in certain coastal and shallow ocean areas that some of the data ICESat-2 should have been collecting were not present in the data, because the onboard receiver algorithms were limiting the downlinked data. The missed bathymetry could hinder study of nearshore and shallow water environments and preclude discovery of previously unknown features, such as geologic/geomorphic structures, reefs, sandbars, or seamounts. Based on these discoveries and with input from the science community, the ICESat-2/ATLAS Flight Science Receiver Algorithms team have performed two algorithm parameter updates with the goal of enhancing ATLAS's bathymetric measurement capability.

ICESat-2's enhanced bathymetric capability, enabled by the algorithm parameter changes, has the potential to benefit a wide range of scientific disciplines, including coastal geomorphology, marine ecology, marine archaeology, hydrography, and oceanography. This paper details the algorithm changes that enable ICESat-2's enhanced bathymetric capability, followed by a rigorous investigation of the achieved bathymetric improvements at local and global scales. We implemented a two-phased experiment, with the first phase focused on site-specific analysis and the second focused on investigating the global impacts of ICESat-2's enhanced bathymetric capability. The results show that the parameter adjustments substantially improve bathymetric data acquisition, eliminate data gaps, and approximately double ICESat-2's global bathymetric coverage area.

2 Materials and Methods

2.1 Flight Receiver Algorithm Updates

The ICESat-2/ATLAS Flight Science Receiver Algorithms include algorithms for on-board signal processing and selection of data to telemeter (i.e., to transmit to ground stations). The receiver algorithms were designed with several adjustable parameters that were initially established pre-launch, but that could be modified on-orbit to satisfy data volume considerations and improve specific data acquisition for a variety of science disciplines. These parameters are specified in three sets of files, one for each of the Photon Counting Electronics cards (PCEs). Since launch, several updates have been made to the parameters, often at the request of the scientific community. However, an important constraint is that parameter adjustments cannot cause the data volume limit to exceed 577.4 Gb/day (McGarry et al., 2019, 2021).

The algorithm parameter updates that were undertaken to enhance ATLAS's bathymetric measurement performance were both designed to modify the telemetry window. This window can be envisioned as a vertical band, centered approximately at the height of the Earth's surface. The upper limit of the telemetry window establishes the height above the Earth's surface at which photon returns start to be recorded in the telemetered data, and the lower limit establishes the depth below the surface at which they cease to be recorded. In this way, the window performs an analogous function to a "range gate" in airborne lidar. The tradeoff in setting these limits is that, if the window is too large, the amount of telemetered data will increase, potentially exceeding the data volume limit; however, if it is too narrow, or not centered correctly, important features of the Earth's surface can be missed in the recorded data. It is important to note that bathymetric photons are detected by ATLAS from a wide range of depths regardless of the telemetry window settings, but that the telemetry window settings truncate the data that are downlinked.

The telemetry band limits are calculated with an on-board Digital Relief Map (DRM), along with additional scaling, padding and offset parameters. The DRM is a set of 0.25° grid cells, with maximum relief calculated at 140 m and 700 m length scales, compiled from best-available relief data (Leigh et al., 2015). The scaling, padding and offset parameters vary by beam strength and surface type which is determined by the on-board Surface Reference Mask (SRM). The SRM is a set of 0.25° grid cells that determine the surface type (land ice, sea ice, land, or ocean) used by the receiver algorithms for signal processing (McGarry et al., 2019). To determine the telemetry band limits, first, the relief in the DRM is scaled to ensure the full span of the surface elevations is within the telemetry band. For land and land ice, a scale factor of 2 is used, while for ocean and sea ice, the scale factor is 1. Next, a padding parameter is applied to the scaled relief as a buffer to compensate for potential inaccuracies in the DRM. Lastly, an offset is applied to shift the telemetry band up or down in vertical space around the expected surface. For a complete description of the on-board databases and calculating the telemetry band size and limits, see McGarry et al. (2019). In the receiver algorithm parameter files, the parameters relating to the telemetry band limits are in units of time (round trip travel time of light), with 10 ns increments. For ease of interpretation in this paper, we convert the parameter values and resulting telemetry band widths to elevations with units of meters by multiplying by the speed of light and dividing by 2 to account for the round-trip travel time. The standard geolocation algorithms use the speed of light in air (standard atmosphere) and we report the main telemetry band heights. However, because the speed of light slows in water, we also add a parenthetical value that show the actual depth after refraction correction using speed of light in water (e.g., (-18 m refraction corrected)).

The goal of the algorithm parameter changes was to optimize the telemetry window for recording bathymetry, subject to operational constraints. The primary focus was on the lower bound of the telemetry window, which is especially important for bathymetry (Figure 1). If it is too close to the water surface (i.e., too shallow), then bathymetry that ICESat-2 ATLAS is otherwise capable of measuring will not be recorded. The updated parameter values were informed by published research on ICESat-2 bathymetry and recommendations of the ICESat-2 Bathymetry Working Group. The first receiver algorithm parameter update for bathymetry (Version 10) served to increase bathymetry acquisition in the open ocean. Previously, the ocean telemetry bands generally spanned ±24 (+24/-18 m refraction corrected) from the sea surface (Figure 2a). It was determined that extending the previous lower limit of the telemetry window from -24 m (-18 refraction corrected) below the surface down to -54 m (-41 m refraction corrected) would be sufficient to capture the maximum depth for nearly all Jerlov coastal water types, based on ATLAS's maximum depth measurement capabilities (Jerlov, 1976; Williamson & Hollins, 2022).

To create the desired telemetry band over the ocean, the vertical padding was increased by 15 m to 39 m, and a vertical offset of 15 m was applied. Utilizing the offset parameter resulted in the additional vertical padding extending the telemetry band deeper below the apparent surface while leaving the above surface limit unchanged. This allowed for a smaller padding increase to reach the desired limits, minimizing the impact on the data volume. These changes were applied to only the three strong spots and affect all ocean telemetry bands, and not just areas with possible bathymetry. The weak spots are less likely to produce bathymetric returns, and, therefore, no changes were made to the weak spot parameters. These Version 10 updates were successfully implemented on-orbit on January 27, 2021.

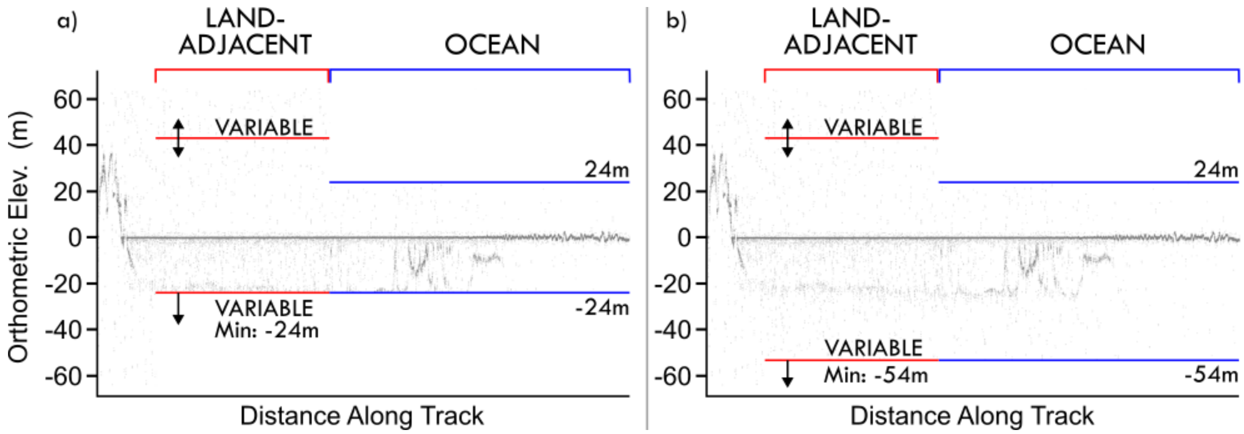

Figure 1. Diagram showing the telemetry window changes, a) before the version 10 (ocean) and 14 (land-adjacent) updates and b) after the version 10 and 14 updates. The red and blue horizontal bars demarcate the vertical extents of the data telemetered from the satellite to the ground stations over land and ocean, respectively. As depicted in (a), before the parameter updates, the lower extent of the telemetry window was too shallow, resulting in missed bathymetry.

While the increased ocean telemetry bands reduced bathymetry clipping, there were still instances along coastlines where bathymetry data was being clipped (Figure 2b and 2c). A DRM tile can contain multiple surface types; however, the algorithms require one surface type to be selected for signal processing. The SRM assigns a single surface type per tile and gives land priority over ocean. Telemetry bands over coastlines therefore use the land parameters and do not have the extended depth applied to ocean telemetry bands.

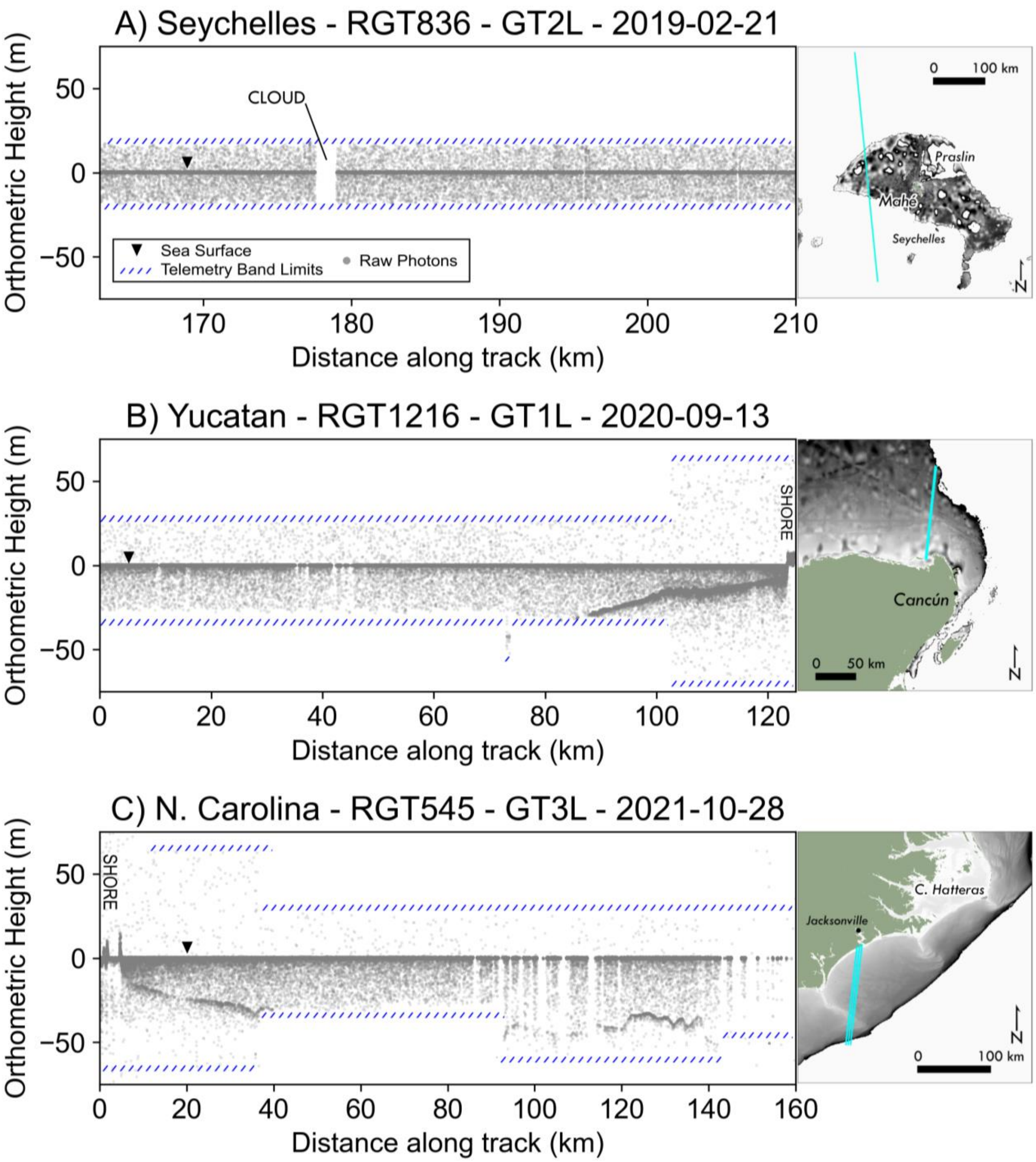

Figure 2. Pre-update ICESat-2 Elevation profile tracks: a) Missing bathymetric data in the Indian Ocean west Mahè island, Seychelles due to the telemetry band limits; b) Bathymetric data loss north of Cancun, Mexico on the Yucatan peninsula; c) Bathymetric data loss near Jacksonville on the coast of North Carolina. The DEM colors in the study area maps are ETOPO elevations from 0 (white) to -60m (black). Note that the y-axis, orthometric heights, are extremely exaggerated, ~400x, compared to the along-track distance values.

To create the desired telemetry for the coastal areas, the minimum padding for land strong spots was increased by 30 m to approximately 54 m (-41 m refraction corrected). This padding applies to all land areas with a DRM relief value of approximately 189 meters or less. The increase in the minimum land padding reduced bathymetry clipping along coastlines where the SRM has not switched from land to ocean by ensuring those bands reach at least -54 m (-41 m after refraction correction). Due to the variable nature of the relief and, thus, the padding parameters for land, the adjustments for coastline bathymetry could not use the same padding and offset method as the ocean adjustments described above. The land adjustments also have minimal implications to both data volume and data quality. The Version 14 changes were not applied to the weak spots, to remain consistent with the previous ocean update (Version 10) for capturing bathymetry.

2.2 Impacts of the telemetry window updates

We used a two-phased approach to investigate and quantify ICESat-2's enhanced bathymetric capability enabled by these algorithm parameter changes. Our goal for the first phase was to perform site-specific analyses enabling a detailed investigation of the enhancement in bathymetry retrieval at local scales. In this phase, we selected sites with varying seafloor morphologies, substrates, and cover types and with gaps in bathymetric coverage appearing for different reasons (Version 10 vs. Version 14). Georeferenced and refraction-corrected (Parrish et al., 2019) seafloor returns from the pre- and post-algorithm parameter changes were compared to investigate their impacts. For one of the sites, the new ICESat-2 bathymetry enabled by the algorithm parameter updates was compared against a reference digital elevation model. In the second phase of the study, we focused on investigating the impacts of the algorithm parameter updates at a global scale. This was performed using the best-available (although coarse) global water clarity and bathymetric data to quantify the global area of potential new bathymetry gained via the algorithm parameter changes.

2.2.1 Site Specific Analysis of telemetry window updates

In selecting sites for the first phase of the study (site-specific analysis), we sought locations that were representative of: a) different seafloor morphologies and substrate/cover types, and b) different reasons for missing or clipped data in ICESat-2 bathymetry derived from data collected before the algorithm parameter changes. Based on these criteria, three sites were selected: 1) offshore of Mahé Island, Seychelles, in the western Indian Ocean (Figure 2a); 2) north of the barrier island of Isla Holbox, in the Yucatan, Mexico (Figure 2b); and 3) offshore of Frying Pan Shoals east and south of Cape Fear, North Carolina, USA (Figure 2c). The Mahé Island site is part of the Seychelles Archipelago, containing fringing reefs with skeletal carbonate and terrigenous sediments (Lewis, 1968) the primary Jerlov water type at this site is IB. The Yucatan site consists of low-gradient continental shelf extending into the Gulf of Mexico and is characterized as microtidal tide regime (Medellín & Torres-Freyermuth, 2019) and Jerlov water type ranging from 9C to IB. The North Carolina site extends south from the barrier islands near North Topsail Beach along the broad continental shelf toward Frying Pan Shoals south of Cape Fear. This stretch of the North Carolina coast is characterized as a wave-dominated barrier coast with mixed semidiurnal tides with a mean range of ~1 m (Hasbrouck, 2007; NOAA, 2023) and a range of Jerlov water types from 5C to IB. The nearshore morphology is characterized by rippled scour depressions and a range of substrates from mud to medium-grained sand to rock outcrop (Thieler, 1996). The site is frequently impacted by hurricanes and nor'easters.

For the first phase of the study, we obtained ATL03 geolocated photon clouds from the NASA National Snow and Ice Data Center Distributed Active Archive Center (NSIDC DAAC) for dates before and after the telemetry window updates (Neumann et al., 2023). The beam tracks over the

Seychelles were exact repeats over an area west of Mahé Island. For North Carolina and the Yucatan, we chose the closest beam tracks between the two dates to minimize any spatial differences between the two profiles. Water surface and seafloor point labeling were done manually and the refraction correction methods are described in Parrish et al. (2019).

The geolocated photon clouds for the three sites before the telemetry window parameter changes are shown in Figure 2. In the Seychelles (Figure 2a), the original telemetry window resulted in missed bathymetry below the -24 m (-18 m refraction corrected) cut-off. The northern Yucatan site, Figure 2b, also shows bathymetry clipping from 0 - 90 km along track caused by the land/ocean telemetry band transition. In Figure 2c, on the coast of North Carolina, the telemetry band switching between land and ocean settings caused the bathymetry from 40 - 90 km along track to be clipped.

2.2.2 Assessment of Global Coastal Bathymetry Retrievability

The global analysis used monthly climatology (2017-2022) diffuse attenuation coefficient at 490 nm (Kd490) from the Visible Infrared Imaging Radiometer Suite (VIIRS) instrument aboard the NOAA-20 (formerly JPSS-1) satellite (NASA OB.DAAC, 2022), and ETOPO2022 global relief model elevations (NOAA-NCEI, 2022) for water clarity and bathymetry estimates, respectively. A key consideration in the use of these datasets was their relatively coarse spatial resolutions and accuracies. The VIIRS Kd490 datasets have 0.04° (~4 km) resolution. However, the VIIRS Kd490 algorithms (Wang et al., 2009) include a semi-analytical technique designed for coastal waters and were found in a previous study (Forfinski-Sarkozi & Parrish, 2016) to be suitable for similar ICESat-2 bathymetric feasibility analysis. Meanwhile, the ETOPO2022 dataset is an amalgamation of the ‘best available’ data sources, which includes inputs of widely ranging resolutions and accuracies. For large areas of the global oceans, ETOPO2022 is based on the GEBCO 2022 dataset which comprises approximately 71.8% “indirect measurements", such as depths “predicted based on satellite-derived gravity data” (47.2%) and “Interpolated based on a computer algorithm” (23.2%) (GEBCO Compilation Group, 2022). Importantly, however, in nearshore areas ETOPO incorporates higher-resolution, better-accuracy data, where available; hence, the quality of the data is generally better in the areas of greatest interest for our purposes. Ultimately, we determined that both global datasets were sufficient for the global analysis portion of the study. Our global analysis does not account of ICESat-2’s beam footprint (~11 m per spot) on individual overpasses and instead focuses on where bathymetry could be retrieved globally given ICESat-2’s 91-day repeat cycle and off pointing capability.

The methodology used to estimate the amount of new bathymetry that might be available to ICESat-2 globally is illustrated in Figure 3. The monthly climatology data was resampled from ~4 km pixel resolution to 30 arc-seconds (~900 m) resolution via bilinear interpolation to match the other datasets. The resampled Kd490 raster data was then converted to the diffuse attenuation coefficient for 532 nm wavelength (Kd532) to match ICESat-2’s green wavelength laser system via Eq. 1 (Lu et al., 2016). While no exact conversion between Kd and Secchi depth is possible, numerous empirical relationships have been developed. Employing a widely-used relationship from the field of airborne bathymetric lidar, we converted Kd532 to approximate Secchi depths via Eq. 2 (Guenther, 1985)

$$Kd_{532} = 0.68\,(Kd_{490} - 0.022\,) + 0.054 \qquad (1)$$

$$Z_{sd} = \frac{1.15}{(Kd_{532} - 0.03)} \quad (2)$$

where Kd490 and Kd532 are in inverse meters (m^{-1}) and Z_{sd}, Secchi depth, is in meters. We then compared the calculated Secchi depths to the ETOPO2022 global relief model elevations. The ETOPO20220 elevations are referenced to the Earth Gravitational Model of 2008 (EGM2008) geoid surface, and therefore the negative elevation values in ETOPO2022 are equivalent to depths below EGM08.

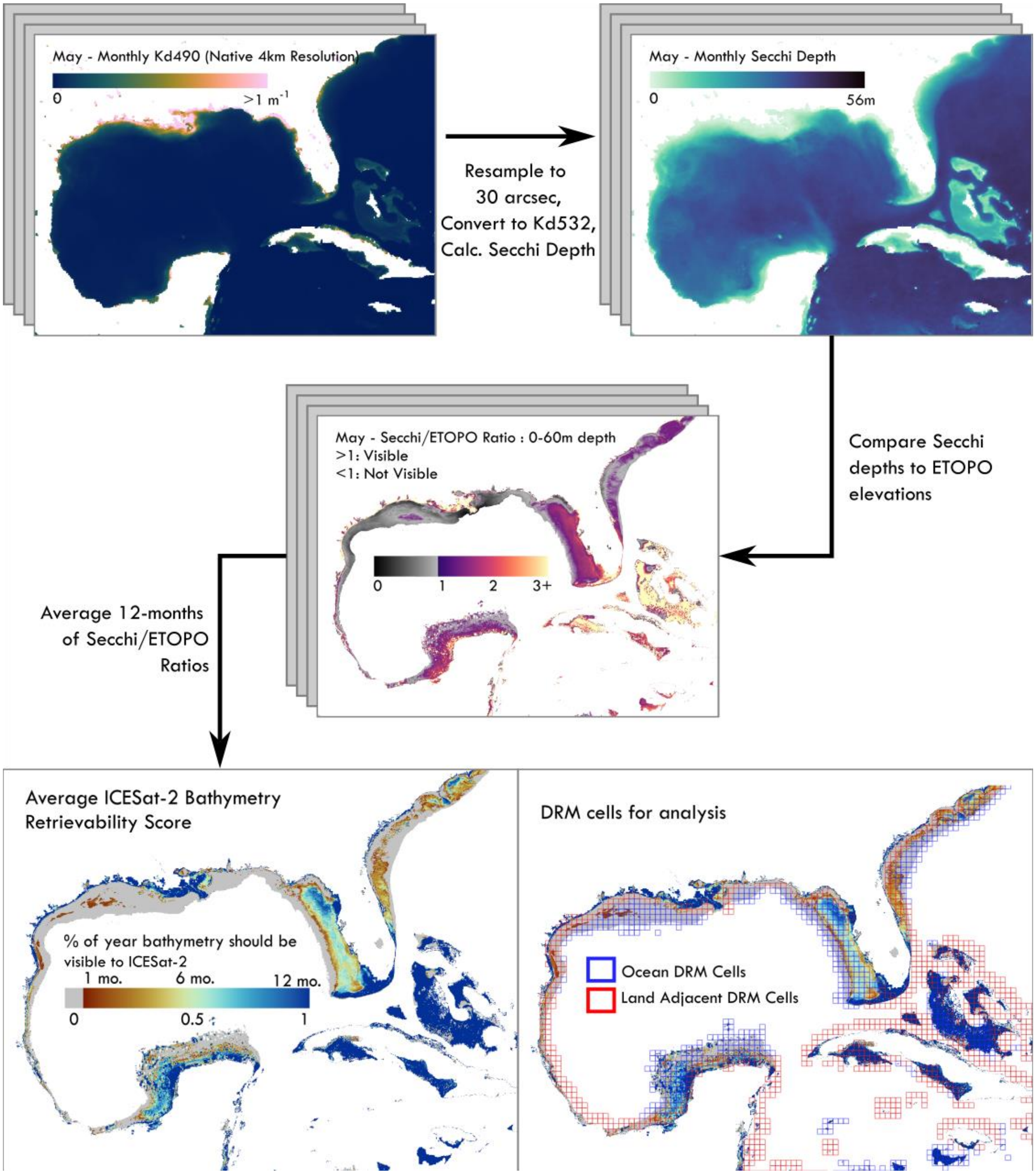

Figure 3. Workflow with example intermediate and final datasets for estimating ICESat-2 bathymetry retrievability from NOAA20-VIIRS Kd490 data.

We next defined and computed a new metric, which we refer to as the extinction depth index, ζ_e:

$$\zeta_e = \frac{Z_{sd}}{Z_{ref}} \qquad (3)$$

where Z_{SD} is the Secchi depth, and Z_{ref} is the reference depth at the same location, with the latter obtained from the ETOPO2022 dataset. Because previous studies have shown that ICESat-

2 is generally capable of bathymetric measurement to ~1 Secchi depth (Parrish et al., 2019; Watkins et al., 2023), the dimensionless ratio (ζ_e) can be thought of as an ICESat-2 bathymetric retrievability index: where $\zeta_e \geq 1$, the seafloor should be detectable by ICESat-2. Next, we calculated an overall score for bathymetric retrievability by: 1) performing a binary reclassification on the monthly extinction depth ratio raster datasets to be one (1) for cells with a ratio greater than or equal to 1.0 and zero (0) for cells less than 1.0; 2) summing the monthly reclassified rasters; and 3) dividing the sum by 12. The retrievability score represents the percentage of an average year that bathymetry would be available for ICESat-2 to measure.

To calculate the total area of the newly available bathymetry we used a zonal statistics operation in QGIS to aggregate statistics from several raster layers into the 0.25° DRM cells. For the Version 10 update, we used open ocean DRM cells and calculated the number of raster cells in the ETOPO2022 raster that were previously available, between 0 and -18 m (refraction corrected) and the number of newly available ETOPO2022 cells between -18 and -41 m (refraction corrected). For the Version 14 update, we used land-adjacent DRM cells where the SRM was previously favoring land parameters, and also calculated the number of newly available ETOPO2022 cells between -18 and -41 m (refraction corrected). The total area was calculated by multiplying the ETOPO cell counts by the square area of the raster pixels, 0.782 km^2.

3 Results and Discussion

3.1 Ocean Parameter Updates

The first parameter updates for enhancing bathymetry acquisition were tested on-orbit for two weeks from November 17 to December 1, 2020. The testing period ensured that the requested adjustments were successfully implemented and that the data volume was minimally affected. After the testing period, the updates concluded successfully and became nominally operational on January 27, 2021. The adjustments made to the ocean parameters were confirmed to have resulted in the lower telemetry band limit extending to at least 54 m below the water surface, for a gain of an additional 30 m.

3.2 Land Parameter Updates

The land parameter updates for enhancing bathymetry acquisition were tested on-orbit for 30 days beginning on November 1, 2022. After the testing period, the updates concluded successfully, and became nominally operational on December 1, 2022. However, there were two instances of activities that caused gaps in the usage of the updated land parameters. Occasionally, the ATLAS Photon Counting Electronics cards (PCEs) for a pair of spots need to be reset. The conditions prompting a reset occurred on PCE1 and PCE3 before the land parameter updates became the default settings. As a result of being reset, PCE1 (spots 1 and 2) did not use the updated parameters from December 29, 2022 to February 6, 2023, and PCE3 (spots 5 and 6) from February 2, 2023 to February 6, 2023. As of February 6, 2023, the updated parameters are the nominal settings for all three PCEs. The land parameter adjustments result in the telemetry band limits along coastlines reaching a minimum of 54 m below the surface for the areas in red in Figure 6a.

3.3 Test Site Profiles

All three sites show new bathymetry in areas that were previously not captured. Figure 3 highlights the changes in the telemetry windows for the Seychelles and Yucatan tracks, before and after the updates. The post-update Seychelles track (Figure 4B) now shows newly available submerged bathymetry below 30 m (~25 m after refraction correction). Specifically, the before-and-after profiles for the Seychelles test site illustrate that after the Version 10 update, new bathymetry was collected within the extended portion of the telemetry bands that would have been missed using the prior ocean parameter setting. The post-update Yucatan track (Figure 4D) shows new bathymetry between 50-95 km along-track in an area that the former telemetry window truncated. The maximum depths reached in the ICESat-2 bathymetry approximately doubled between the pre- and post-update data. Note that clouds and turbidity obscure the near shore bathymetry in this post-update track from ~92-105 km along-track.

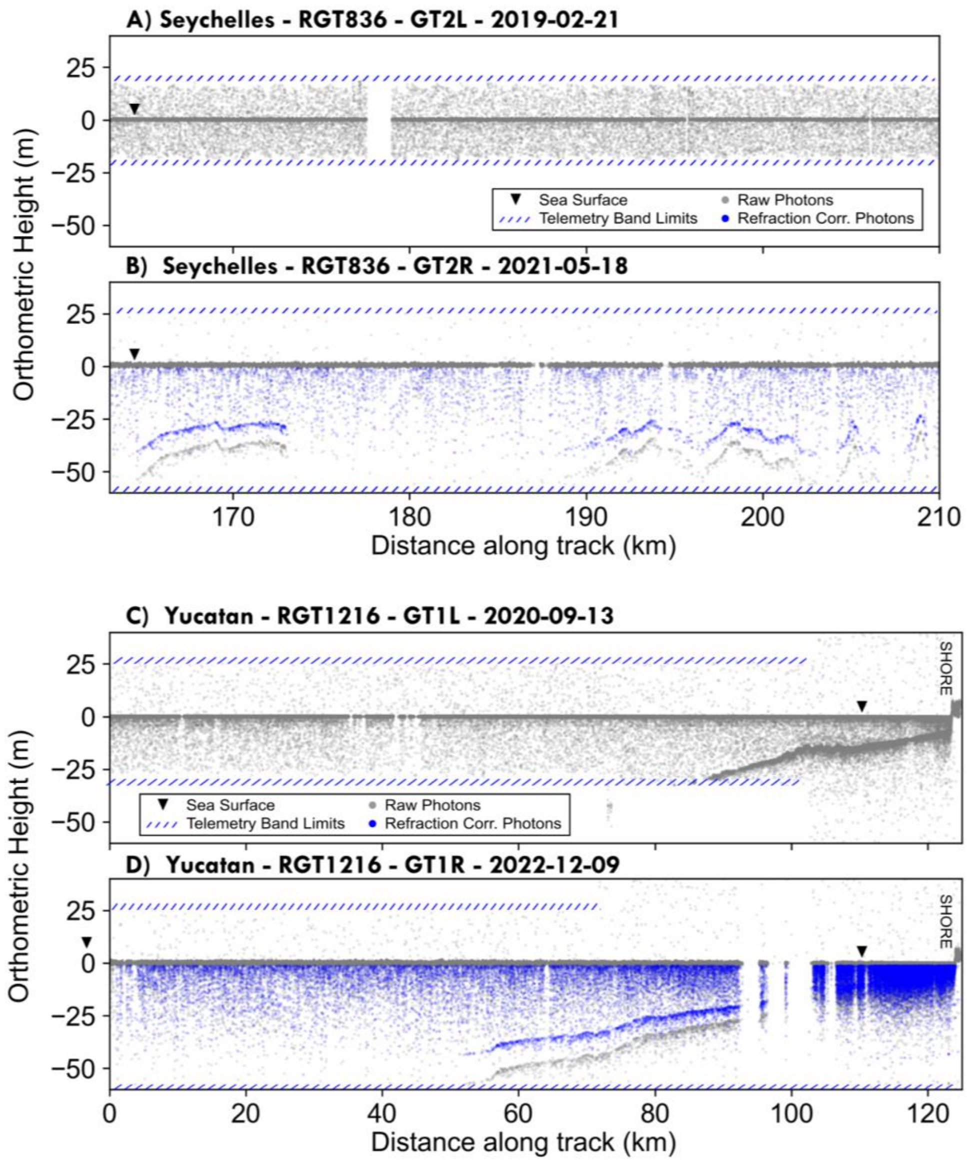

Figure 4. ICESat-2 track profiles illustrating newly available bathymetry: A) Seychelles pre-update profile from Figure 1; B) post-Version 10 update profile for open ocean DRM cells in the Seychelles; C) Yucatan pre-update profile; and D) post-Version 14 update for land-adjacent DRM cells at the Yucatan site.

In North Carolina (Figure 5), ICESat-2's enhanced bathymetric capability allowed for a continuous bathymetric profile from the shore out to 130 km along-track (and potentially more since clouds are blocking returns from 130-160 km along track). Comparing the refraction corrected photon elevations to the CUDEM/ETOT2022 reference elevations, the root mean squared error (RMSE) is 1.17 m. Overall, the refraction corrected photons show excellent correspondence to the reference data. However, there are isolated parts of the profile (e.g., 60 km and 90 km) where the profile deviates from the reference data. The areas contributing to the error metrics are likely due to the different resolution datasets with different accuracies that were used as reference. From 0-60 km along track, the reference data is the 1/9 arc-second CUDEM (3 m cell resolution), 60-118 km is the 1/3 arc-second CUDEM (10 m), and from 118-160 km is the 15-arc-second ETOPO2022 (~460 m).

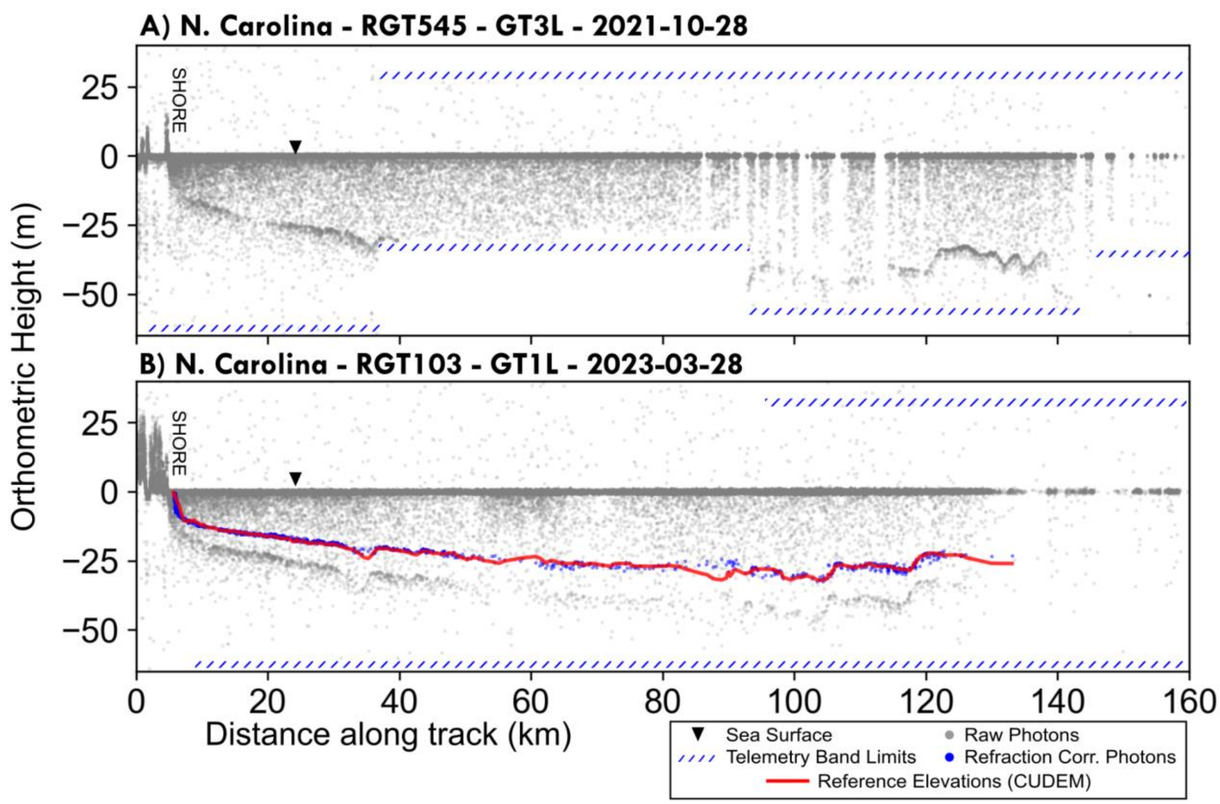

Figure 5. ICESat-2 track profiles illustrating newly available bathymetry at the North Carolina site: A) Pre-update profile and B) post-Version 14 update profile with refraction corrected photons (blue) and CUDEM/ETOPO2022 reference elevations (red).

In areas with newly available bathymetric returns, it is likely that the density of returns from the seabed will be lower because of the exponential attenuation of light in the water column with depth. Future research will be needed to refine algorithms for bathymetric signal finding to accurately detect bathymetry in parts of ICESat-2 profiles that have lower density points. Local atmospheric and ocean conditions can limit the ability of ICESat-2 to collect bathymetry in some areas. Cloudy conditions and obstructions (e.g., sea ice) can completely block ICESat-2 from measuring bathymetry and high local turbidity, large waves, or rough sea conditions will cause increased attenuation and scattering that can limit or preclude photons from returning to ICESat-2.

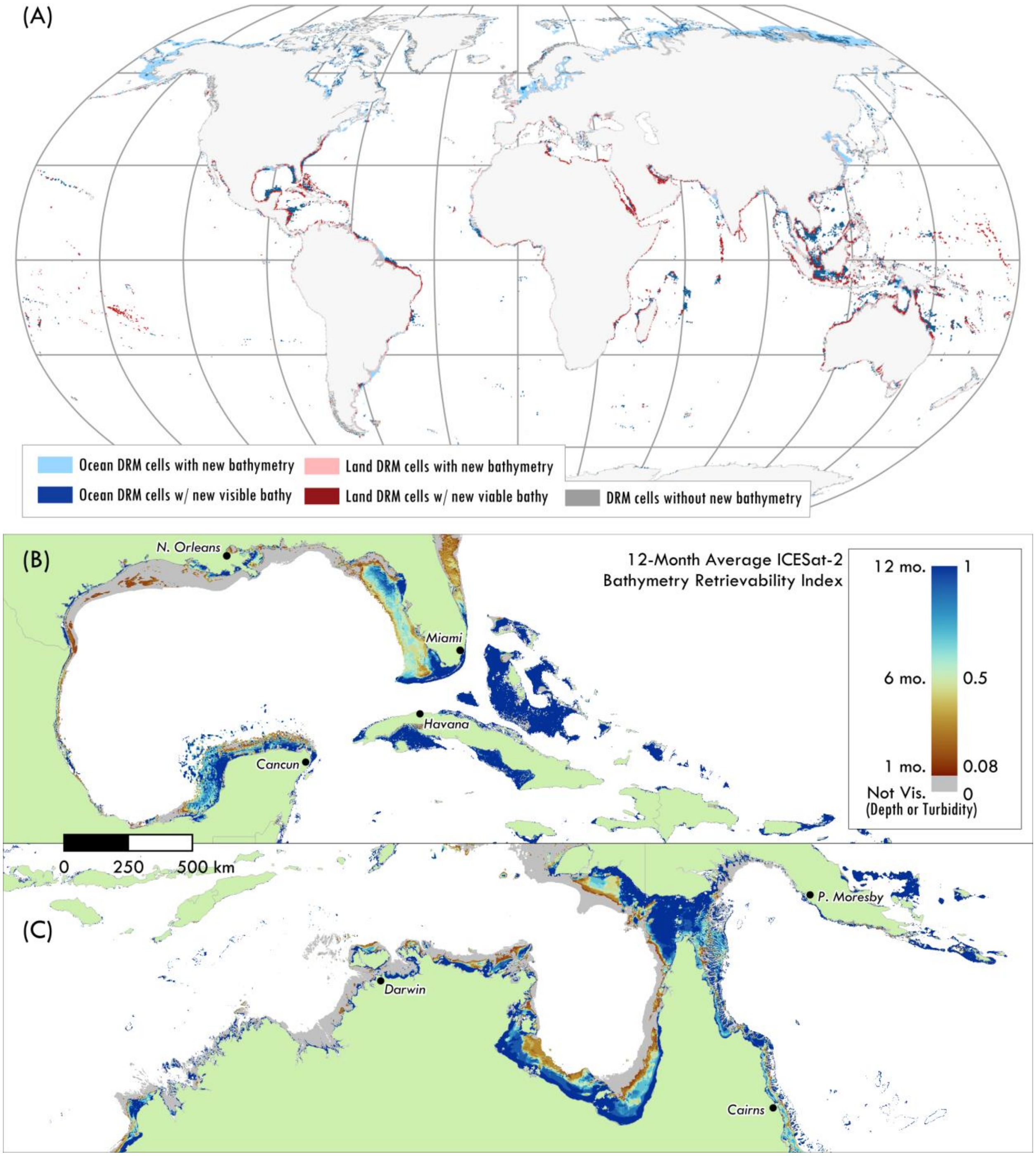

Figure 6. Global bathymetry retrievability. A) Locations where increased telemetry bands allow new bathymetric data acquisition after updates to the parameters corresponding to land-adjacent and ocean DRM tiles. (B and C) Bathymetric retrievability scores based on an average of monthly climatology Kd532 and derived Secchi depths in (B) the Gulf of Mexico/northern Caribbean and (C) northern Australia/Papua New Guinea. A web map version of the 12-month average retrievability index is available in the Data Availability Statement. Monthly raster layers are available in the data release for this paper (Dietrich et al., 2023)

3.4 Extent of newly available bathymetry

Based on our analysis, both receiver algorithm parameter updates approximately double the total area of bathymetry to 13.82 million km^2 that ICESat-2 could potentially detect globally (Table 1 and Figure 6). The potentially available bathymetry in ocean DRM cells (Update 10) increased by 4.93 million km^2 and in the land-adjacent DRM cells (Update 14) increased by 1.18 million km^2. Adding the visibility scores to the analysis of available bathymetry (Figure 5), we found that the total viable bathymetry (areas with at least 1 month of visibility, a retrievability score ≥ 0.08) is a total of 5.65 million km^2. The overall increase over the pre-update bathymetry is ~1.3 million km^2 when we apply the retrievability scores to the bathymetry that was available before the updates.

Table 1. The global area of possible bathymetry that ICESat-2 could potentially detect. Existing bathymetry represents areas unaffected by the updates. Ocean DRM Cells are areas that were affected by the Version 10 update and land-adjacent DRM Cells are areas affected by the Version 14 update.

	Existing	Land-adjacent DRM Cells	Ocean DRM Cells	TOTALS
Pre-Update Bathy Area (km^2)	4,930,500	776,600	2,000,100	**7,707,200**
Pre-Update Area, Visibility ≥ 1 mo. (km^2)	2,736,200	560,000	1,042,500	**4,338,700**
% of Pre-update Area Visible in at least 1 month	55%	72%	52%	**56%**
Post-Update Bathy Area (km^2)	-	1,183,100	4,929,900	**6,113,000**
Post-Update Area, Visibility ≥ 1 mo. (km^2)	-	522,600	785,800	**1,308,400**
% of Post-update Area Visible in at least 1 month	-	44%	16%	**21%**
Total Area of Possible Bathymetry (km^2)	4,930,500	1,959,700	6,930,000	**13,820,200**
Total Area, Visibility Score ≥ 1 month (km^2)	2,736,200	1,082,600	1,828,300	**5,647,100**
% of Total Area Visible in at least 1 month	55%	55%	26%	**41%**

The largest gains in available bathymetry occurred in areas with wide, shallow sloping shelf morphologies, which take advantage of both updates, land-adjacent DRM cells that are contiguous with ocean DRM cells. Steeper coastal topography will also benefit in certain cases, but not as dramatically since some of this bathymetry was already visible in land-adjacent DRM cells before the update. Other significant gains are in areas with completely submerged shallow bathymetry in the open ocean (e.g., atolls, sea mounts, shoals) particularly in the Indian and Pacific Oceans. The large difference in pre- and post-update areas for the ocean DRM cells and the lower total percent visible (16%) (Table 1) is largely due to the shallow areas in the Bering Strait, North Sea, and Arctic Ocean. These areas are in the deeper range of ICESat-2's capability (35-41 m) and the turbidity along with seasonal sea ice make these areas difficult to measure.

Our analysis of available bathymetry has two key limitations. The first is the accuracy of the current generation of global bathymetric datasets. The ETOPO2022 dataset used here is an amalgamation of the 'best available' data sources. For large areas of the global oceans, ETOPO2022 is based on the GEBCO 2022 dataset which comprises approximately 71.8% "indirect measurements", such as depths "predicted based on satellite-derived gravity data" (47.2%) and "Interpolated based on a computer algorithm" (23.2%) (GEBCO Compilation

Group, 2022). The areas of indirect measurements likely have large or unknown errors which can lead to inaccurate seabed elevations. These inaccuracies may cause certain bathymetric areas to be included or excluded from our analysis affecting the total area calculations. The second limitation in our analysis of available bathymetry is that our visibility statistics and retrievability scores are built on averages of monthly climatology Kd490 values, which themselves are long-term averages. Therefore, the visibility and retrievability statistics should be used as a guide for where bathymetry retrieval is most likely since the averages may not represent the conditions on any given day of an ICESat-2 overpass.

4 Conclusions

We discuss the Flight Science Receiver Algorithms parameter updates specific to improving bathymetric data collection of NASA's ICESat-2 mission. The two updates were implemented to make adjustments to the ocean telemetry windows in both open ocean and coastal areas. The updates became nominally operational on January 27, 2021 and February 6, 2023, respectively. We demonstrate these parameter adjustments substantially increase bathymetric retrieval capabilities of ICESat-2 to support near-shore bathymetric mapping efforts. Overall, the updates are a substantial upgrade that increases the amount of available bathymetric data for core ocean science topics such as geomorphic and ecological characterization and hydrodynamic modeling (e.g., storm surge, tidal, sea level rise modeling). The new data also provides opportunities to discover previously unknown seafloor features. By allowing ICESat-2 to see deeper there are opportunities to better adjoin with existing sonar surveys, thereby avoiding data gaps that could hinder science objectives. Being able to junction with, and ideally, overlap ICESat-2 and existing and future hydrographic surveys can eliminate data gaps such as those created by NOAA's Navigable Area Limit Line (NALL) established for safety of survey launches at the 3.5-m depth contour (or further offshore, in presence of rocks, breaking waves or other obstructions).

One limitation is that the results of the global assessment of increased bathymetric coverage carried out in this study cannot be utilized for detailed, site-specific analysis, because it was not designed for this purpose. Specifically, the coarse resolutions and relatively lower spatial accuracies of the global turbidity and bathymetry datasets, especially in shore adjacent pixels, do not permit detailed analysis. Therefore, future work is recommended to carry out similar analyses over local to regional extents, ideally using in situ data (e.g., optical buoy data and boat-based multibeam echosounder data) or higher spatial resolution satellite measurements of Kd. ICESat-2 bathymetry data, especially with the on-going development of a new Level-3A data product for ICESat-2 (designated ATL24), will make automatically processed along-track bathymetry data available globally. This will be a source of direct measurements of bathymetry for inclusion into local and global mapping products, such as ETOPO and GEBCO, increasing the overall accuracy of these products in critical coastal zones. Future research will focus on developing and tuning ATL24 algorithms to best leverage ICESat-2's enhanced bathymetric capability, as well as use of the new bathymetry for assessing nearshore morphological change and benthic habitat change globally.

Acknowledgments

The authors would like to thank the ICESat-2 Bathymetry Working group for many fruitful discussions. The authors declare no real or perceived financial conflicts of interests. Funding for this research was partially provided through a NASA grant 80NSSC22K1878 from the ICESat-2 Project Science Office at Goddard Space Flight Center and through NASA grant 80NSSC22K1102 from the Decadal Survey Incubation program focus on Surface, Topography and Vegetation Science Team (STV).

Open Research

Data Availability Statement:

- The ICESat-2 ATL03 data used in this study are available via the National Snow and Ice Data Center (NSIDC) - nsidc.org (DOI: 10.5067/ATLAS/ATL03.005 Neumann et al., 2021)
- The VIIRS Kd490 data is available via the NASA Ocean Biology DAAC - oceancolor.gsfc.nasa.gov (NASA OB.DAAC, 2022)
- The ETOPO2022 data is available from the NOAA National Centers for Environmental Information - https://www.ncei.noaa.gov/products/etopo-global-relief-model (NOAA NCEI, 2022)
- The web map version of the 12-month retrievability index is available at: https://experience.arcgis.com/experience/474b9d16f9da4ca4b2830fcfa92852d9
- Individual Raster dataset layers are available as part of the data release for this paper DOI: 10.6084/m9.figshare.24570049.v2 (Dietrich et al., 2023)

References

Albright, A., & Glennie, C. (2021). Nearshore Bathymetry From Fusion of Sentinel-2 and ICESat-2 Observations. *IEEE Geoscience and Remote Sensing Letters*, *18*(5), 900–904. https://doi.org/10.1109/LGRS.2020.2987778

Babbel, B. J., Parrish, C. E., & Magruder, L. A. (2021). ICESat-2 Elevation Retrievals in Support of Satellite-Derived Bathymetry for Global Science Applications. *Geophysical Research Letters*, *48*(5), e2020GL090629. https://doi.org/10.1029/2020GL090629

Cao, B., Fang, Y., Gao, L., Hu, H., Jiang, Z., Sun, B., & Lou, L. (2021). An active-passive fusion strategy and accuracy evaluation for shallow water bathymetry based on ICESat-2 ATLAS laser point cloud and satellite remote sensing imagery. *International Journal of Remote Sensing*, *42*(8), 2783–2806. https://doi.org/10.1080/01431161.2020.1862441

Chen, Y., Chen, Y., Zhu, Z., Le, Y., Qiu, Z., Chen, G., et al. (2021). Refraction correction and coordinate displacement compensation in nearshore bathymetry using ICESat-2 lidar data and remote-sensing images. *Optics Express*, *29*(2), 2411–2430. https://doi.org/10.1364/OE.409941

Dietrich, J. T., Rackley-Reese, A., Gibbons, A., Magruder, L. A., & Parrish, C. E. (2023). ICESat-2 Bathymetry Retrievability Index [Data set]. Figshare. https://doi.org/10.6084/m9.figshare.24570049.v2

Forfinski-Sarkozi, N. A., & Parrish, C. E. (2016). Analysis of MABEL Bathymetry in Keweenaw Bay and Implications for ICESat-2 ATLAS. *Remote Sensing*, *8*(9), 772. https://doi.org/10.3390/rs8090772

GEBCO Compilation Group. (2022). GEBCO_2022 Grid [Data set]. https://doi.org/10.5285/e0f0bb80-ab44-2739-e053-6c86abc0289c

Guenther, G. C. (1985). *Airborne laser hydrography : system design and performance factors* (Professional Paper). Rockville, MD: National Ocean Service,Charting and Geodetic Services.

Hasbrouck, E. G. (2007). *The influence of tidal inlet migration and closure on barrier planform changes: Federal Beach, NC* (PhD Thesis). University of North Carolina Wilmington.

Herrmann, J., Magruder, L. A., Markel, J., & Parrish, C. E. (2022). Assessing the Ability to Quantify Bathymetric Change over Time Using Solely Satellite-Based Measurements. *Remote Sensing*, *14*(5), 1232. https://doi.org/10.3390/rs14051232

Jerlov, N. G. (1976). *Marine Optics*. Elsevier.

Le Quilleuc, A., Collin, A., Jasinski, M. F., & Devillers, R. (2022). Very High-Resolution Satellite-Derived Bathymetry and Habitat Mapping Using Pleiades-1 and ICESat-2. *Remote Sensing*, *14*(1), 133. https://doi.org/10.3390/rs14010133

Leigh, H. W., Magruder, L. A., Carabajal, C. C., Saba, J. L., & McGarry, J. F. (2015). Development of Onboard Digital Elevation and Relief Databases for ICESat-2. *IEEE Transactions on Geoscience and Remote Sensing*, *53*(4), 2011–2020. https://doi.org/10.1109/TGRS.2014.2352277

Lewis, M. S. (1968). The Morphology of the Fringing Coral Reefs along the East Coast of Mahé, Seychelles. *The Journal of Geology*, *76*(2), 140–153. https://doi.org/10.1086/627319

Lu, X., Hu, Y., Pelon, J., Trepte, C., Liu, K., Rodier, S., et al. (2016). Retrieval of ocean subsurface particulate backscattering coefficient from space-borne CALIOP lidar measurements. *Optics Express*, *24*(25), 29001–29008. https://doi.org/10.1364/OE.24.029001

Ma, Y., Xu, N., Liu, Z., Yang, B., Yang, F., Wang, X. H., & Li, S. (2020). Satellite-derived bathymetry using the ICESat-2 lidar and Sentinel-2 imagery datasets. *Remote Sensing of Environment*, *250*, 112047. https://doi.org/10.1016/j.rse.2020.112047

Markus, T., Neumann, T., Martino, A., Abdalati, W., Brunt, K., Csatho, B., et al. (2017). The Ice, Cloud, and land Elevation Satellite-2 (ICESat-2): Science requirements, concept, and implementation. *Remote Sensing of Environment*, *190*, 260–273. https://doi.org/10.1016/j.rse.2016.12.029

McGarry, J. F., Carabajal, C., Degnan, J., Holland, S. T., Mallama, A., Palm, S., et al. (2019). *ATLAS Flight Science Receiver Algorithms* (No. GSFC-E-DAA-TN72602). Retrieved from https://ntrs.nasa.gov/citations/20190031952

McGarry, J. F., Carabajal, C. C., Saba, J. L., Reese, A. R., Holland, S. T., Palm, S. P., et al. (2021). ICESat-2/ATLAS Onboard Flight Science Receiver Algorithms: Purpose, Process, and Performance. *Earth and Space Science*, *8*(4), e2020EA001235. https://doi.org/10.1029/2020EA001235

Medellín, G., & Torres-Freyermuth, A. (2019). Morphodynamics along a micro-tidal sea breeze dominated beach in the vicinity of coastal structures. *Marine Geology*, *417*, 106013. https://doi.org/10.1016/j.margeo.2019.106013

NASA OB.DAAC. (2022). Visible and Infrared Imager/Radiometer Suite (VIIRS) Level-3 Mapped Downwelling Diffuse Attenuation Coefficient, Version 2022. NASA Goddard Space Flight Center, Ocean Ecology Laboratory, Ocean Biology Processing Group, Greenbelt, MD, USA. https://doi.org/10.5067/NOAA-20/VIIRS/L3M/KD/2022

Neuenschwander, A., & Pitts, K. (2019). The ATL08 land and vegetation product for the ICESat-2 Mission. *Remote Sensing of Environment*, *221*, 247–259. https://doi.org/10.1016/j.rse.2018.11.005

Neumann, T. A., Martino, A. J., Markus, T., Bae, S., Bock, M. R., Brenner, A. C., et al. (2019). The Ice, Cloud, and Land Elevation Satellite – 2 mission: A global geolocated photon product derived from the Advanced Topographic Laser Altimeter System. *Remote Sensing of Environment*, *233*, 111325. https://doi.org/10.1016/j.rse.2019.111325

Neumann, T. A., Brenner, A., Hancock, D., Robbins, J., Saba, J., Harbeck, K., et al. (2021). ATLAS/ICESat-2 L2A Global Geolocated Photon Data, Version 5 [Data set]. NASA National Snow and Ice Data Center Distributed Active Archive Center. https://doi.org/10.5067/ATLAS/ATL03.005

Neumann, T. A., Brenner, A., Hancock, D., Robbins, J., Gibbons, A., Lee, J., et al. (2023). ATLAS/ICESat-2 L2A Global Geolocated Photon Data, Version 6 [Data set]. NASA National Snow and Ice Data Center Distributed Active Archive Center. https://doi.org/10.5067/ATLAS/ATL03.006

NOAA. (2023). Wrightsville Beach, NC Tide Gauge (Station ID: 8658163) [Data set]. Retrieved from https://tidesandcurrents.noaa.gov/stationhome.html?id=8658163

NOAA National Centers for Environmental Information. (2022). ETOPO 2022 15 Arc-Second Global Relief Model [Data set]. https://doi.org/10.25921/fd45-gt74

Parrish, C. E., Magruder, L. A., Neuenschwander, A. L., Forfinski-Sarkozi, N., Alonzo, M., & Jasinski, M. (2019). Validation of ICESat-2 ATLAS Bathymetry and Analysis of ATLAS's Bathymetric Mapping Performance. *Remote Sensing*, *11*(14), 1634. https://doi.org/10.3390/rs11141634

Ranndal, H., Sigaard Christiansen, P., Kliving, P., Baltazar Andersen, O., & Nielsen, K. (2021). Evaluation of a Statistical Approach for Extracting Shallow Water Bathymetry Signals from ICESat-2 ATL03 Photon Data. *Remote Sensing*, *13*(17), 3548. https://doi.org/10.3390/rs13173548

Schutz, B. E., Zwally, H. J., Shuman, C. A., Hancock, D., & DiMarzio, J. P. (2005). Overview of the ICESat Mission. *Geophysical Research Letters*, *32*(21). https://doi.org/10.1029/2005GL024009

Selamat, M. B., Muhiddin, A. H., Yusuf, S., & Jompa, J. (2021). Toward geomorphic mapping of reef habitat by laser altimeter on ICESat-2 Satellite. *IOP Conference Series: Earth and Environmental Science*, *860*(1), 012080. https://doi.org/10.1088/1755-1315/860/1/012080

Thieler, E. R. (1996). Shoreface Processes in Onlsow Bay. In W. J. Cleary (Ed.), *Environmental Coastal Geology: Cape Lookout to Cape Fear* (pp. 19–29). Carolina Geological Society. Retrieved from https://carolinageologicalsociety.org/1990s_files/gb%201996s.pdf#page=76

Thomas, N., Lee, B., Coutts, O., Bunting, P., Lagomasino, D., & Fatoyinbo, L. (2022). A Purely Spaceborne Open Source Approach for Regional Bathymetry Mapping. *IEEE Transactions on Geoscience and Remote Sensing*, *60*, 1–9. https://doi.org/10.1109/TGRS.2022.3192825

Van An, N., Quang, N. H., Son, T. P. H., & An, T. T. (2023). High-resolution benthic habitat mapping from machine learning on PlanetScope imagery and ICESat-2 data. *Geocarto International*, *38*(1), 2184875. https://doi.org/10.1080/10106049.2023.2184875

Wang, M., Son, S., & Harding Jr., L. W. (2009). Retrieval of diffuse attenuation coefficient in the Chesapeake Bay and turbid ocean regions for satellite ocean color applications. *Journal of Geophysical Research: Oceans*, *114*(C10). https://doi.org/10.1029/2009JC005286

Watkins, R. H., Sayers, M. J., Shuchman, R. A., & Bosse, K. R. (2023). Validation of ICESat-2 Derived Data Products on Freshwater Lakes: Bathymetry, Diffuse Attenuation Coefficient for Downwelling Irradiance (Kd), and Particulate Backscatter Coefficient (bbp). *IEEE Geoscience and Remote Sensing Letters*, *20*, 1–5. https://doi.org/10.1109/LGRS.2023.3261551

Williamson, C. A., & Hollins, R. C. (2022). Measured IOPs of Jerlov water types. *Applied Optics*, *61*(33), 9951–9961. https://doi.org/10.1364/AO.470464

Zhang, D., Chen, Y., Le, Y., Dong, Y., Dai, G., & Wang, L. (2022). Refraction and coordinate correction with the JONSWAP model for ICESat-2 bathymetry. *ISPRS Journal of Photogrammetry and Remote Sensing*, *186*, 285–300. https://doi.org/10.1016/j.isprsjprs.2022.02.020

Figure and Table Captions

Figure 1. Diagram showing the telemetry window changes, a) before the version 10 (ocean) and 14 (land-adjacent) updates and b) after the version 10 and 14 updates. The red and blue horizontal bars demarcate the vertical extents of the data telemetered from the satellite to the ground stations over land and ocean, respectively. As depicted in (a), before the parameter updates, the lower extent of the telemetry window was too shallow, resulting in missed bathymetry..

Figure 2. Pre-update ICESat-2 Elevation profile tracks: a) Missing bathymetric data in the Indian Ocean west Mahè island, Seychelles due to the telemetry band limits; b) Bathymetric data loss north of Cancun, Mexico on the Yucatan peninsula; c) Bathymetric data loss near Jacksonville on the coast of North Carolina. The DEM colors in the study area maps are ETOPO elevations from 0 (white) to -60m (black). Note that the y-axis, orthometric heights, are extremely exaggerated, ~400x, compared to the along-track distance values.

Figure 3. Workflow with example intermediate and final datasets for estimating ICESat-2 bathymetry retrievability from NOAA20-VIIRS Kd490 data.

Figure 4. ICESat-2 track profiles illustrating newly available bathymetry: A) Seychelles pre-update profile from Figure 1; B) post-Version 10 update profile for open ocean DRM cells in the Seychelles; C) Yucatan pre-update profile; and D) post-Version 14 update for land-adjacent DRM cells at the Yucatan site.

Figure 5. ICESat-2 track profiles illustrating newly available bathymetry at the North Carolina site: A) Pre-update profile and B) post-Version 14 update profile with refraction corrected photons (blue) and CUDEM/ETOPO2022 reference elevations (red).

Figure 6. Global bathymetry retrievability. A) Locations where increased telemetry bands allow new bathymetric data acquisition after updates to the parameters corresponding to land-adjacent and ocean DRM tiles. (B and C) Bathymetric retrievability scores based on an average of monthly climatology Kd532 and derived Secchi depths in (B) the Gulf of Mexico/northern Caribbean and (C) northern Australia/Papua New Guinea. A web map version of the 12-month average retrievability index is available in the Data Availability Statement. Monthly raster layers are available in the data release for this paper (Dietrich et al., 2023)

Table 1. The global area of possible bathymetry that ICESat-2 could potentially detect. Existing bathymetry represents areas unaffected by the updates. Ocean DRM Cells are areas that were affected by the Version 10 update and land-adjacent DRM Cells are areas affected by the Version 14 update